

DETECTION OF SEPARATRICES AND CHAOTIC SEAS BASED ON ORBIT AMPLITUDES

JÉRÔME DAQUIN AND CAROLINA CHARALAMBOUS

ABSTRACT. The Maximum Eccentricity Method (MEM, [17]) is a standard tool for the analysis of planetary systems and their stability. The method amounts to estimating the maximal stretch of orbits over sampled domains of initial conditions. The present paper leverages on the MEM to introduce a sharp detector of separatrices and chaotic seas. After introducing the MEM analogue for nearly-integrable action-angle Hamiltonians, *i.e.*, diameters, we use low-dimensional dynamical systems with multi-resonant modes and junctions, supporting chaotic motions, to recognise the drivers of the diameter metric. Once this is appreciated, we present a second-derivative based index measuring the regularity of this application. This quantity turns to be a sensitive and robust indicator to detect separatrices, resonant webs and chaotic seas. We discuss practical applications of this framework in the context of N -body simulations for the planetary case affected by mean-motion resonances, and demonstrate the ability of the index to distinguish minute structures of the phase space, otherwise undetected with the original MEM.

CONTENTS

1. Introduction	1
2. Action-diameter applied to resonant models	3
2.1. Models and numerical settings	4
2.2. Application to the integrable pendulum	4
2.3. Application to slow chaos of a modulated pendulum	5
2.4. Application to resonance overlap	6
3. The $\ \Delta D\ $ indicator	7
4. Application to planetary problems	8
4.1. Generalities and numerical setups	9
4.2. The 2-planet case	10
4.3. The 3-planet case	10
5. Conclusions	12
Appendix A. Application to a discrete case	12
Appendix B. Analytical properties of the diameter for the pendulum model	14
Acknowledgments	15
References	15

1. INTRODUCTION

Among the 5,000 discovered extrasolar systems¹, there is a great diversity in multiplicities of planets and central stars, orbital architectures (spacing between planets, orbital parameters), or physical properties (masses, radii). Being able to understand the complex gravitational interactions

Date: December 6, 2022.

Key words and phrases. Maximum eccentricity method; Stability maps; Dynamical indicator; Mean-motion resonances; Planetary systems .

¹Confer The Extrasolar Planets Encyclopaedia, <http://exoplanet.eu> [54].

of this kaleidoscope, such as the dynamics associated to resonant configurations, is a dynamical challenge that help to retrace their histories since formation, and further constrain observational campaigns (see, *e.g.*, [26, 30, 6, 59, 58]). The Maximum Eccentricity Method (hereafter, MEM) introduced by [17] originated to probe the dynamical structure and largeness of stability regions of exoplanetary systems in the context of direct numerical integrations of the equations of motion. By denoting an orbital element set $\alpha = (a, e, i, \Omega, \omega, M)$ where a denotes the semi-major axis, e the eccentricity, i the inclination, Ω the longitude of the ascending node, ω the argument of perigee and M the mean-anomaly, the MEM index assigns, for an admissible initial condition α_0 , the maximal stretch of the orbital eccentricity over a finite time window $[0, t]$, $t \in \mathbb{R}_+$:

$$(1) \quad \delta e(\alpha_0; t) = \max_{0 \leq \tau \leq t} e(\tau) - \min_{0 \leq \tau \leq t} e(\tau).$$

For short, and to follow conventional notations, we drop the initial datum α_0 and time t from Eq. (1) to simply note δe . The time window is problem dependent, and is chosen in accordance with the dynamical or physical timescales. The MEM has been used in a variety of contexts and across distinct scales, ranging from the study of near-Earth space artificial satellite dynamics [27, 2, 1, 16, 53] up to the resonant structure of satellites around giant planets [7], including the stability of planetary systems [17, 34, 3]. Depending on the dynamical context, it might be more appropriate to substitute Eq. (1) by its analogue

$$(2) \quad \delta a(\alpha_0; t) = \max_{0 \leq \tau \leq t} a(\tau) - \min_{0 \leq \tau \leq t} a(\tau).$$

In using Eq. (2) over Eq. (1), as *e.g.*, in the context of mean-motion resonances [23] or tesseral effects with the Earth [11], a dynamical understanding of the problem is injected into the computed quantity (in both cases, the semi-major axis is the variable primarily excited by the perturbation). The δe or δa indices are most typically used in the context of dynamical maps where the scalars are colour-coded accordingly to their magnitudes, and computed over 2-dimensional grid of initial conditions (*i.e.*, a δe or δa heatmap is computed by “freezing” 4 variables in the initial datum α_0). As a matter of fact, the computation of the amplitudes (diameters) is a useful tool in delineating and visualising dynamical structures of multidimensional problems. This paper extends the MEM capabilities and reports an existing connection with chaos identification. In fact, we present a simple method to unravel sharply dynamical structures and chaotic seas from the knowledge of orbits only and MEM like computations, yielding to a robust and sensitive non-variational chaos indicator.

We would like to stress that the reported method does not constitute a “new branch” of chaos indicator (among which it is customary to distinguish between frequential like methods (*e.g.*, [36]), or variational methods such as the the Fast Lyapunov Indicator (FLI) and variations [22, 21, 4], the MEGNO [10], the SALI [56] or GALI [57] indices, to name but a few), but is instead thoroughly related to the Lagrangian Descriptor (LD) framework in which the M -function assigning euclidean length² to orbits plays a central role [40, 43, 41]. In fact, paraphrasing [41], it is clear from Eqs. (1) and (2) that δe and δa are actually positive quantities that accumulate along the trajectory, one of the cornerstone property behind LDs. LDs have been precious allies over the years for gaining dynamical understandings in a variety of contexts and range of fields, such as the detection of Lagrangian coherent structures in geophysical and oceanic flows (see *e.g.*, [43, 13, 14]), but also and especially in the field of reaction dynamics in theoretical chemistry, allowing to recover stable and unstable manifolds of normally hyperbolic invariant manifolds (NHIM) in a non-perturbative approach (see *e.g.*, [12, 20, 33, 46]). Recently, two non-variational chaos indicators have been proposed in concert from the M -function by [15] and [32]. The present paper follows closely the steps

²The LD framework does not rely exclusively on the euclidean norm. In this respect, p -norm like LDs [38], LDs based on the actions in the context of Hamiltonians framework [24], or time-free geometrical LDs for integrable problems [48] have been considered in several instances.

of [15] by recognising the resemblance of the M -function with MEM like quantities used in orbital settings.

The rest of the paper is organised as follows:

- In Sect. 2, we introduce the MEM general counterpart in the setting of n degree-of-freedom (DoF) action-angle Hamiltonian. The introduced quantity corresponds to a diameter, D , measuring the maximal amplitude of the actions over a finite time window. The diameter metric is then studied over slices of initial conditions on paradigmatic models of resonances, supporting possibly chaotic motions. These include the integrable pendulum model, the modulated pendulum with a thin chaotic layer, and a two-waves Hamiltonian model where resonances overlap. The analysis leads to a better understanding of the dynamical drivers of the diameter.
- In Sect. 3, we introduce a scalar quantity encoding the regularity of the diameter metric. The index, denoted $\|\Delta D\|$, is based on the evaluation of the second derivatives of D . This quantity is a sensitive and robust scalar able to detect sharply hyperbolic trajectories and multi-resonant modes. It is proposed as a new non-variational chaos indicator.
- In Sect. 4, in the context of N -body simulations, we apply our framework to the 2 and 3 bodies planetary problem. In this case, the diameter metric reduces to the original MEM like quantity given in Eq. (2), δa . We demonstrate the benefits of considering $\|\Delta \delta a\|$ over δa to restore the separatrices of the 2 planet problem, and resonant templates of mean-motions configurations in the 3 planet case. The $\|\Delta \delta a\|$ offers details of the phase space otherwise unseen with the δa quantity.

We close the paper by summarising our results and main contributions.

2. ACTION-DIAMETER APPLIED TO RESONANT MODELS

In order to extend the MEM to the more general setting of n -DoF Hamiltonian written in action-angle variables (I, ϕ) in $\mathbb{R}^n \times \mathbb{T}^n$, we find convenient to introduce the *diameter* of an orbit. This follows the direction and terminology employed by [28] in the context of nearly-integrable maps (see complimentary results on the formalism developed in Appendix A). Let us denote by \mathcal{D} a subset of $\mathbb{R}^n \times \mathbb{T}^n$. For a given initial condition (I_0, ϕ_0) in \mathcal{D} , we define the diameter metric as³

$$(3) \quad \begin{aligned} D : \mathcal{D} \times \mathbb{R} &\rightarrow [0, +\infty), \\ (I_0, \phi_0; t) &\mapsto D(I_0, \phi_0; t), \end{aligned}$$

with

$$(4) \quad D(I_0, \phi_0; t) = \left\| (\delta I_1(I_0, \phi_0; t), \dots, \delta I_n(I_0, \phi_0; t)) \right\|_\infty,$$

³We shall not consider here blowing-up trajectories in finite-time. We thus assume to deal with bounded observables, leading to a finite diameter D . In the N -body simulations of Sect. 4, escapes in finite time are not excluded. Nevertheless, we bypass this problem by using conditional exit loops during the numerical treatment of the equation of motions. This prevents the issue to happen. Equivalently, it amounts in some cases to consider the final time variable as a function of the initial datum, $t = t(I_0, \phi_0)$.

where each element of the set $\{\delta I_j(I_0, \phi_0; t)\}_{j=1}^n$, represents the amplitude⁴ of the considered action⁵:

$$(5) \quad \delta I_j(I_0, \phi_0; t) = \max_{0 \leq \tau \leq t} I_j(I_0, \phi_0, \tau) - \min_{0 \leq \tau \leq t} I_j(I_0, \phi_0, \tau), \quad j = 1, \dots, n.$$

To avoid notation burden, we shall not distinguish between the D metric or its value (the diameter, noted D) provided an initial datum. It is clear from Eqs. (4) and (5) that the D metric is an increasing function of time, accumulating a positive scalar along the orbit's history. We analyse now how the D metric behaves on low-dimensional resonant models.

2.1. Models and numerical settings. We consider the following three archetypal resonant models

$$\begin{cases} \mathcal{H}(I, \phi) = \frac{I^2}{2} - \cos \phi, & (I, \phi) \in \mathcal{C}, \mathcal{C} = \mathbb{R} \times [0, 2\pi], \\ \mathcal{J}(I, \phi, t) = \frac{I^2}{2} - (1 + \alpha \cos \epsilon t) \cos \phi, & (I, \phi, t) \in \mathcal{C} \times \mathbb{R}, \\ \mathcal{K}(I, \phi, t) = \frac{I^2}{2} - (\alpha_1 \cos(\phi - t) + \alpha_2 \cos(\phi + t)), & (I, \phi, t) \in \mathcal{C} \times \mathbb{R}, \end{cases}$$

where $\epsilon \ll 1$, $\alpha < 1$, α_1, α_2 are real positive parameters. For each model, described further in the subsequent, we compute values of D over chosen slices of initial conditions. In order to evaluate Eq. (3), we have fixed the time window to $\mathcal{T} = [0, 500]$. The non-autonomous models have been converted into 2-DoF autonomous models by extending the dimension of the phase space through the introduction of canonical variables (J, τ) , where $\dot{\tau}$ has a trivial dynamics. As the ‘‘dummy’’ action J has no dynamical relevance, the diameter D is computed only by monitoring the action I (*i.e.*, we compute a one dimensional diameter corresponding to the amplitude of the action I). Although the pendulum model \mathcal{H} is 1-DoF with a phase space easily described by the level-set method (see further discussions on analytical properties of D in Appendix B), all the corresponding flows have been numerically approximated using numerical solvers.

2.2. Application to the integrable pendulum. The well-known phase space of the 1-DoF pendulum model \mathcal{H} on $\mathcal{D} \times [-\pi, \pi]$, $\mathcal{D} \subset \mathbb{R}$, obtained by the level-set method is shown in the left frame of Fig. 1. The phase space contains the three fixed points, the stable equilibrium at the origin $(\phi, I) = (0, 0)$ and the fixed points $(\phi, I) = (\pi, 0) = (-\pi, 0)$. The level curve associated to the energy $E = 1$ of the hyperbolic equilibrium, *i.e.*, the separatrix (shown as a red curve), divides orbits of the phase space with distinct qualitative behaviours. Within the cat-eye domain ($E < 1$), the phase space is foliated by librational curves, whilst outside the cat-eye region ($E > 1$), circulatory tori enclose the cylinder. The half-width δI of the resonance, *i.e.*, the distance between $I = 0$ and the apex of the separatrix, satisfies

$$(6) \quad \mathcal{H}(0, \delta I) = 1.$$

Solving this last equation for δI , one find $\delta I = 2$ leading, by symmetry, to the full resonant width $\Delta I = 2\delta I = 4$. The right companion panel of Fig. 1 shows the landscape of the D metric computed as a function of the initial action I for the fixed angle $\phi = 0$ (corresponding to the vertical dashed blue line in the phase space of the pendulum). For $I \geq 0$, the D function grows linearly within

⁴Interestingly enough, we shall underline that similar definitions based on amplitudes in certain direction found applications in fluid mechanics for characterising mixing properties, see [44].

⁵Note that Eqs. (1) and (2) are not based directly on actions, yet, the metrical orbital elements (a, e, i) are simple function of proper actions such as the Delaunay elements (L, G, H) , for example. Thus, large variations in a are equivalent to large variations in $L = \sqrt{\mu a}$, and, in the secular approximation where L is a first integral, large variations in e are equivalent to large variations in $G = L\sqrt{1 - e^2}$.

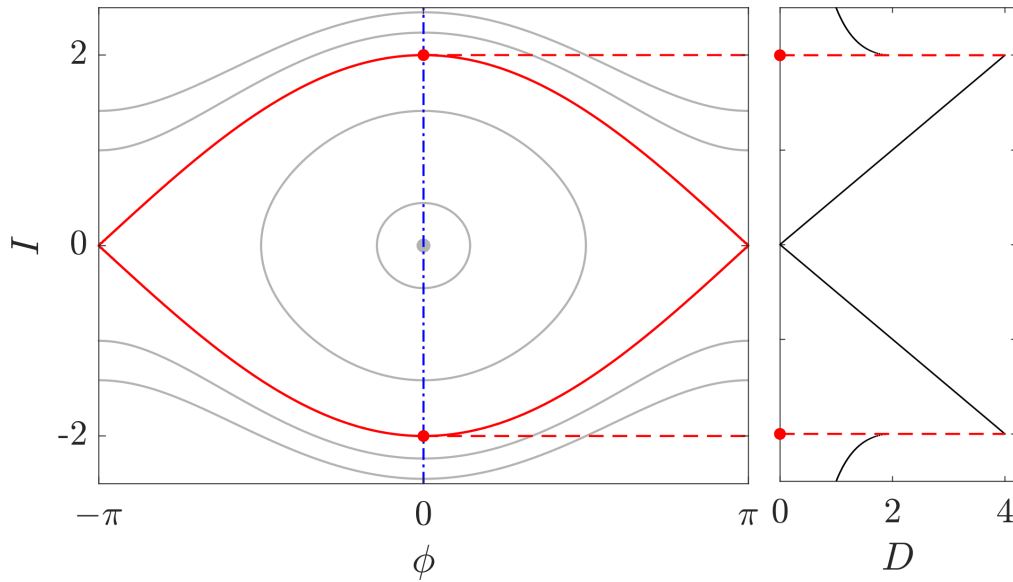


FIGURE 1. (Left) Phase space of the pendulum model \mathcal{H} with the cat-eye separatrix topology (red). (Right) Landscape of the diameter D computed over the dashed blue line of initial conditions for fixed $\phi = 0$ and varying I ranging the circulatory and librational domains. The red horizontal lines materialise the actions corresponding to the separatrix crossing. At those values, D is discontinuous.

the librational domain up to the apex of the separatrix (corresponding to the action $I = 2$). The crossing of the separatrix is materialised by a sudden loss of continuity in the D function. At this point, D is only left-continue and reaches its maximal value, $D(2) = \Delta I = 4$. For $I > 2$, the graph decreases monotonically. A similar picture is obtained by symmetry for $I < 0$. From the numerical estimation of D , one infer that D is not differentiable at $I = 0$, and $I = \pm 2$ (where the function is not even continuous). Those properties of the D metric are proven analytically in Appendix B.

2.3. Application to slow chaos of a modulated pendulum. The 2-DoF autonomous version of \mathcal{J} , still denoted \mathcal{J} , reads

$$(7) \quad \mathcal{J} = \frac{I^2}{2} + \epsilon J - (1 + \alpha \cos \tau) \cos \phi.$$

As the time variable τ is slow ($\dot{\tau} = \epsilon$, $\epsilon \ll 1$), this model is paradigmatic of slow chaos where 3 resonances are ϵ -close [18]. In fact, using trigonometrical identities, \mathcal{J} might be written as

$$(8) \quad \mathcal{J} = \frac{I^2}{2} + \epsilon J - \left(\cos \phi + \frac{\alpha}{2} \cos(\phi - \tau) + \frac{\alpha}{2} \cos(\phi + \tau) \right),$$

where the 3 harmonics are clearly apparent, and ϵ apart. Indeed, using Hamilton's canonical equations, one sees that the centres of the resonances $\dot{\phi} = 0$, $\dot{\phi} - \dot{\tau}$ and $\dot{\phi} + \dot{\tau}$ correspond respectively to the actions values $I = 0$, $I = \epsilon$, $I = -\epsilon$. Iterations of the stroboscopic mapping computed for the numerical values $\alpha = 0.25$, $\epsilon = 0.1$, and obtained by projecting in the (I, ϕ) plane snapshots of the flow at times t such that $\epsilon t = 0 \pmod{2\pi}$, are shown in the left panel of Fig. 2. The (I, ϕ) phase space contains predominantly regular curves, and a stochastic layer surrounding the unperturbed separatrix. In fact, in the limit $\epsilon \rightarrow 0$, the outer and inner boundaries of the chaotic sea can be related to instantaneous separatrices associated to integrable approximations of \mathcal{J} by freezing the time related variable [18]. The D landscape, computed for $(J, \phi, \tau) = 0$, is similar to the landscape of the pendulum model. The most noticeable difference occurs for the range of actions crossing

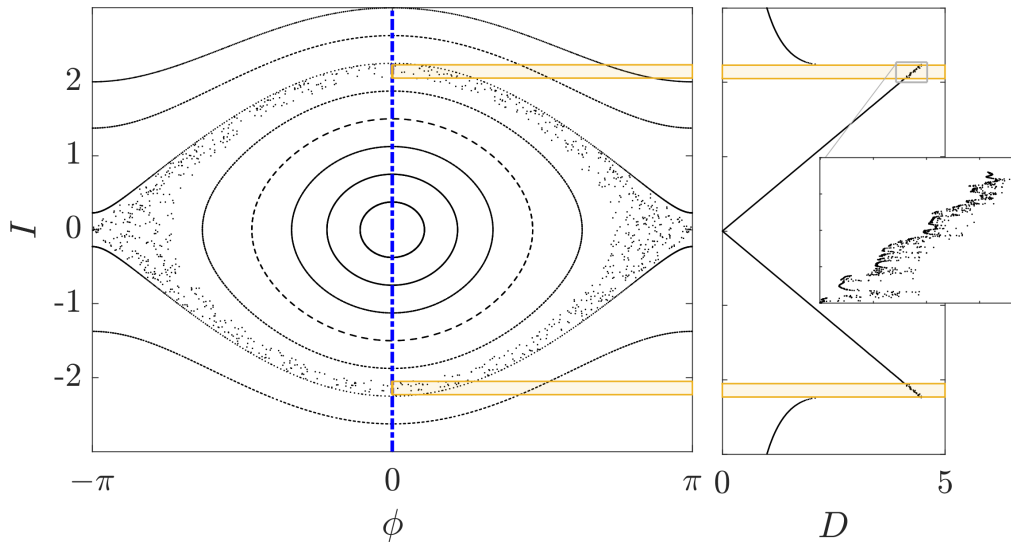


FIGURE 2. (Left) Phase space of the modulated pendulum \mathcal{J} , using $\alpha = 0.25$ and $\epsilon = 0.1$, obtained by iterating the period-map. (Right) Landscape of the diameter D computed over the dashed blue line of initial conditions. The range of the chaotic layer are delineated with the slightly transparent filled areas. It establishes a link between the loss of regularity of D and the crossing of the hyperbolic region. The inlaid panel shows a zoomed in portion of D when crossing the chaotic layer.

the hyperbolic layer, for which the D metric loses its regularity, as seen in the two-scales plot in the right panel of Fig. 2.

2.4. Application to resonance overlap. The 2-DoF autonomous counterpart of \mathcal{K} reads

$$(9) \quad \mathcal{K} = \frac{I^2}{2} + J - (\alpha_1 \cos(\phi - \tau) + \alpha_2 \cos(\phi + \tau)).$$

When $\alpha_1 = 0$ or $\alpha_2 = 0$, we recover the integrable Hamiltonian of the pendulum using an ad-hoc canonical change of variables. The phase space then contains a single cat-eye resonance centred around either $c_1 = -1$ or $c_2 = 1$, with half-widths $\delta_2 = 2\sqrt{\alpha_2}$ or $\delta_1 = 2\sqrt{\alpha_1}$ respectively. Whenever both α_1 and α_2 are different from zero, the 2-DoF Hamiltonian is no longer integrable [19]. The resonance overlap parameter, also called *stochasticity parameter* [9, 42], reads

$$(10) \quad s = \frac{\delta_1 + \delta_2}{|c_2 - c_1|} = \sqrt{\alpha_1} + \sqrt{\alpha_2}.$$

In our numerical setting, we assign to each resonant eye the same dynamical weight with $\alpha_1 = \alpha_2 = 1/5$, leading to $s \approx 0.89$. As s is close to 1, the resonances overlap significantly and macroscopic chaos is expected. Iterations of the stroboscopic map, obtained by projecting the flow in the (I, ϕ) plane for times t such that $t = 0 \pmod{2\pi}$, are shown in the left panel of Fig. 3 for $I \geq 0$. The phase space contains a large connected chaotic sea. The remnants of the librational domains contains several chains of periodic orbits surrounded by thin chaotic layers. The observation made before on the regularity of the D -metric when crossing hyperbolic tangles is made more evident, as illustrated in the right panel of Fig. 3. The landscape of the D metric contains the characteristic V-shape already observed when crossing elliptical regions, and becomes irregular for actions leading to hyperbolic motions.

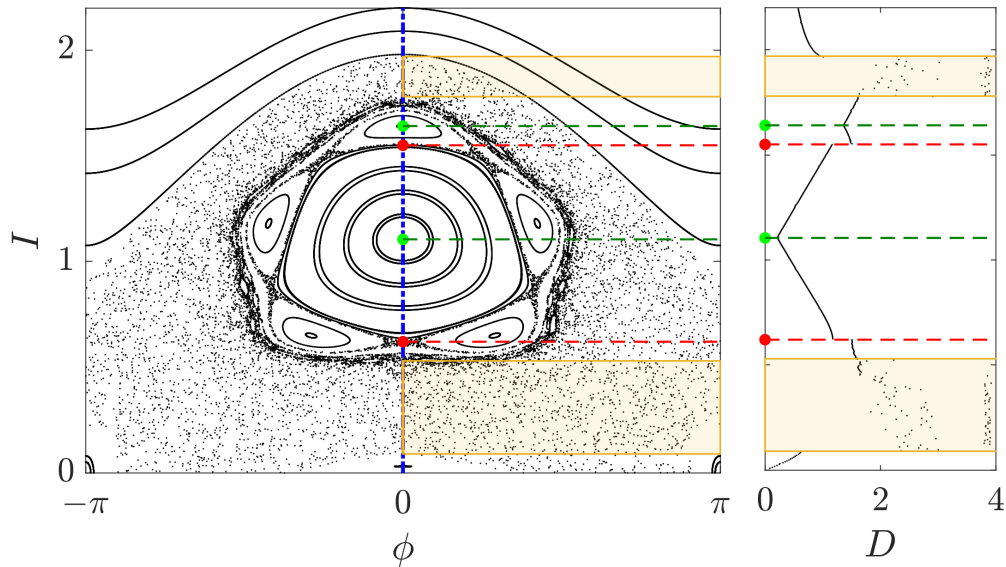


FIGURE 3. (Left) Phase space of the two-waves Hamiltonian \mathcal{K} , with $\alpha_1 = \alpha_2 = 1/5$, obtained by iterating the period-map. (Right) Landscape of the diameter D computed over the dashed-blue line of initial conditions.

3. THE $\|\Delta D\|$ INDICATOR

As computationally just observed, the diameter metric encapsulates signatures of relevant dynamical information, however, the latter are not encoded into the final value of D but rather in the regularity of the application. This is reminiscent of properties of the M -function [41]. This observation, however, conflicts with the current use of the diameter to visualise dynamical structures, especially in the context of stability maps. Albeit we are not able to provide a general proof, based on the former observations, we conjecture the D metric to be non differentiable when crossing transversally hyperbolic domains. This property offers the possibility of delineating sharply hyperbolic domains by quantifying instead the regularity of the application. In this respect, following the same strategy of the frequency analysis [36], we find convenient to introduce the second-order derivative based quantity

$$(11) \quad \|\Delta D(I_0, \phi_0; t)\| = \sum_{i=1}^n \left| \partial_{I_0^{(i)}}^2 D(I_0, \phi_0; t) \right|,$$

where $I_0^{(i)}$ denotes the i -th component of the initial datum I_0 .

Remark 1. *In the following, the diameters D are estimated numerically using discretised domains of initial conditions. We compute Eq. (11) using central differences. For the sake of simplicity, assume we are evaluating D as a function of $I \in \mathcal{I} = [i_{\min}, i_{\max}] \subset \mathbb{R}$. We evaluate D for each action $I_j = i_{\min} + jh$, with $h = (i_{\max} - i_{\min})/N$, N being a sufficiently large natural number fixing the resolution of the mesh. The numerical approximation of Eq. (11), for points in $\tilde{\mathcal{I}}$ reads*

$$(12) \quad \frac{\partial^2 D(I_j)}{\partial I^2} \simeq \frac{D(I_{j+1}) + D(I_{j-1}) - 2D(I_j)}{h^2}.$$

This procedure is generalised to higher dimensional domains of initial conditions, e.g., for sections $\Sigma \subset \mathbb{R}^2$, as schematically represented in Fig. 4.

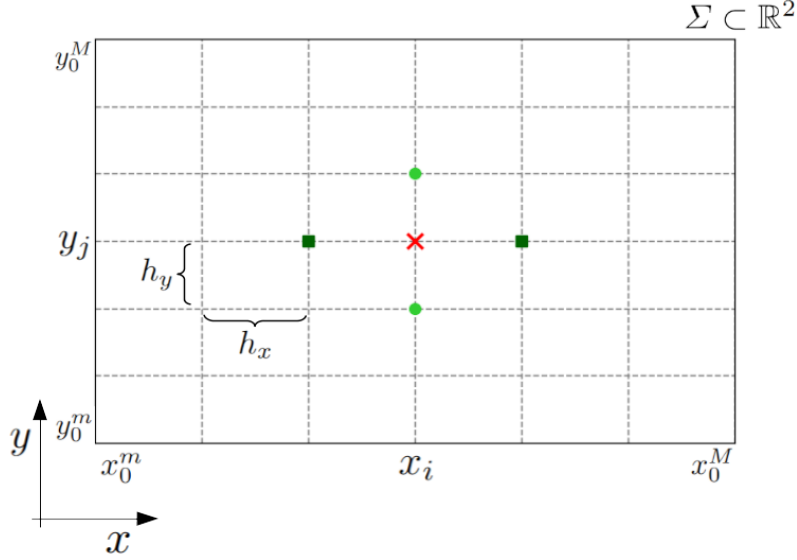


FIGURE 4. Schematic representation of the approach taken to estimate the $\|\Delta D\|$ index through the second derivatives appearing in Eq. (11) when the computation is performed on a 2-dimensional section Σ . For a point $(x_i, y_j) \in \dot{\Sigma}$ (cross), besides the value of the diameter at the point (x_i, y_j) itself, the second derivatives are estimated using the 4 neighbouring values at the points $x_{\pm} = x_i \pm h_x$ (diamonds) and $y_{\pm} = y_j \pm h_y$ (circles), accordingly to Eq. (12). The couple (h_x, h_y) define the resolution of the Cartesian mesh obtained as $h_x = (x_0^M - x_0^m)/N_x$ and $h_y = (y_0^M - y_0^m)/N_y$. Typical values to produce a resolved map are $N_x = N_y = 500$.

Fig. 5 presents a heatmap of the diameter associated to the pendulum model (a similar computation is performed by [52]), and its associated $\|\Delta D\|$ landscape computed for varying I and fixed $\phi = 0$ (dashed vertical line). The points leading to the largest diameters correspond to librational orbits whose energy approaches the energy associated to the separatrix (where $D \sim 4$). This leads to a map where the vicinity of the separatrix (within the librational domain) takes approximately the same diameter values. Instead, the $\|\Delta D\|$ landscape reacts as sharp Dirac impulses for the actions corresponding to the separatrix ($I = \pm 2$). The values taken by $\|\Delta D\|$ are in fact several orders of magnitude larger than the values associated to the diameters of others librational or circulatory orbits. The only exception appears in the vicinity of the stable equilibria at $I = 0$, where a Dirac pic can also be distinguished, with a lower amplitude though. This observation is consistent with the V-shape of the diameter near the stable equilibria (confer Fig. 1) and the analytical estimates presented in Appendix B.

The next section demonstrates further the benefits of supplementing the D analysis with the $\|\Delta D\|$ index in a practical planetary context.

4. APPLICATION TO PLANETARY PROBLEMS

We now return to the early roots of the MEM grounded in gravitational problems where we apply our apparatus into an N -body framework, namely the 2 and the 3 planet cases. This section demonstrates the ability of the $\|\Delta D\|$ indicator to reveal separatrices and thin details of resonant webs in the context of dynamical maps.

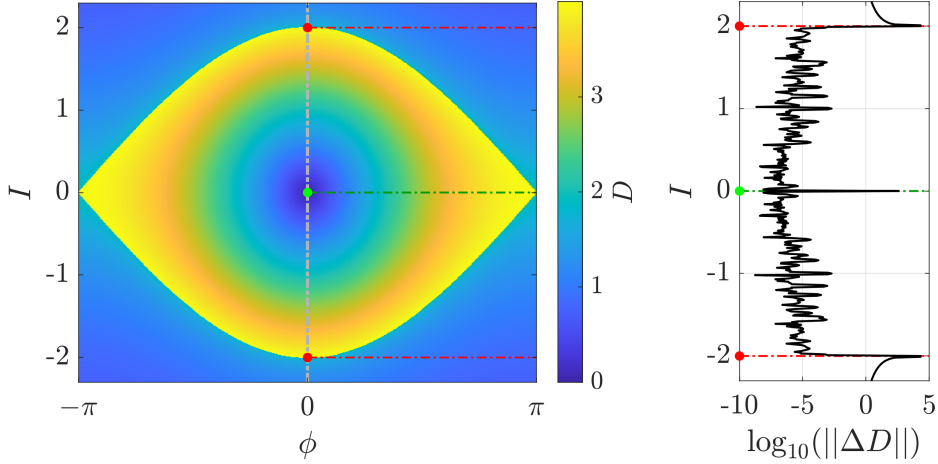


FIGURE 5. Diameter stability map associated to the pendulum model and its corresponding $\|\Delta D\|$ landscape computed along the line $\phi = 0$ (black dashed black line). The $\|\Delta D\|$ metric allows to sharply detect the separatrix crossing, contrarily to the diameter which take similar values in its whole neighbourhood (with $D \simeq 4$). The dashed red lines at $I = \pm 2$ and the dashed green line at $I = 0$ in the landscape materialise the locations of the hyperbolic and stable equilibria respectively, where $\|\Delta D\|$ now reacts as net impulses.

4.1. Generalities and numerical setups. Our dynamical system consists in N_{pl} coplanar planets with masses m_i , $i = 1, \dots, N_{\text{pl}}$, orbiting a central star with mass $M_\star = 1 M_\odot$ where $M_\star \gg m_i$. We study the orbital evolution of the planets with a set of orbital elements α_i as defined in the introduction, with the sub-index referring to planet i in the system. In terms of the modified Delaunay canonical variables [35],

$$(13) \quad \begin{cases} L_i = m_i \sqrt{\mu_i a_i}, & \lambda_i = M_i + \omega_i, \\ S_i = L_i \left(1 - \sqrt{1 - e_i^2}\right), & -\varpi_i = -\omega_i, \end{cases}$$

the system is described by the Hamiltonian function

$$(14) \quad \mathcal{H} = - \sum_{i=1}^{N_{\text{pl}}} \frac{\mu_i m_i^3}{2L_i^2} + \sum_{\mathbf{k}} c_{\mathbf{k}}(\mathbf{L}, \mathbf{S}) \cos(\mathbf{k} \cdot \boldsymbol{\phi})$$

where $\mu_i = \mathcal{G}(M_\star + m_i)$, \mathcal{G} denotes the gravitational constant and (\mathbf{L}, \mathbf{S}) denotes the vectors whose components are (L_i, S_i) , similarly to $\boldsymbol{\phi} = (\boldsymbol{\lambda}, -\boldsymbol{\varpi})$, and $\mathbf{k} \in \mathbb{Z}_\star^{2N_{\text{pl}}}$. The first term in Eq. (14) is the integrable part that refers to the unperturbed Keplerian motion of the planets around the central star. The second term is the perturbing function which accounts for the interactions between the planets. The $c_{\mathbf{k}}$ coefficients in the perturbing function depend on the Laplace coefficients and can be computed from the expressions given in [45]. Our system is thus a $2N_{\text{pl}}$ -DoF problem.

In a general manner, a 3-planet mean-motion resonance (MMR) can be expressed in planetary orbital parameters as

$$(15) \quad k_1 n_1 + k_2 n_2 + k_3 n_3 = 0,$$

where n_i is the mean motion of planet i , and $k = (k_1, k_2, k_3) \in \mathbb{Z}_\star^3$. The coefficient $s = |k_1 + k_2 + k_3|$ is the order of the resonance. The order of a 2-body MMR is known to be the order at which the

eccentricity of the bodies appear in the coefficients of the expansion of the perturbing function. In the case of a 3-body resonance the property still holds, and thus we can separate 3-body resonances into zeroth order ($q = 0$), and non-zero order ($q \neq 0$). The particular case of the 2-planets resonant dynamics is straightforward to describe from the previous expression. A resonance between planets m_1 and m_2 can be described from Eq. (15) when $k_3 = 0$, a resonance between planets m_2 and m_3 , corresponds to $k_1 = 0$, while the last possible 2-planet MMR is between the non adjacent planets, when $k_2 = 0$. In the following, we perform N -body simulations using the code as described by [5]. As a general description, for each case we choose a representative plane, and generate a grid of initial conditions that we integrate for a fixed amount of time. In both scenarios, all angles are set to zero.

4.2. The 2-planet case. Although the pendulum model described in Sect. 2.2 allows for analytical estimations of many of the properties of the MMRs, the Second Fundamental Model of resonance of [31] is more adequate to reproduce the dynamical features in the 2-planet case for planets in circular orbits. Recalling that two planets are in a $(p + q)/p$ MMR with $p, q \in \mathbb{Z}_*$ if the mean motions n_1 and n_2 of the planets satisfy $(p + q)n_2 - pn_1 \sim 0$ and at least one of the associated resonant angles $\phi_{1,2} = (p + q)\lambda_2 - p\lambda_1 - q\varpi_{1,2}$ librates around a fixed value, the resonant dynamics of two planets on eccentric orbits in a MMR of arbitrary order q can be reduced to a 1-DoF Hamiltonian and described with a pendulum like structure (see *e.g.*, [55, 29]). Here we will not write explicitly this procedure, but let us mention that it is possible to derive analytically the location of the fixed points and the separatrix. Instead, we perform brute-force N -body simulations to estimate the main features of the system. MMR affects primarily the semi-major axis observables, and we thus rely on estimating δa , such that Eq. (4) becomes

$$(16) \quad \delta a = \max(\delta a_1, \delta a_2).$$

Focusing on the vicinity of the first-order $n_1/n_2 = 2/1$ MMR, Fig. 6 shows composite results of both the δa and $\|\Delta\delta a\|$ analyses in the representative $(a_1/a_2, e_1)$ plane, constructed over a grid of 500×500 initial conditions integrated for 5×10^3 years. The planetary masses are chosen equal to 0.05 and 0.1 masses of Jupiter, m_{Jup} .

The top left panel of Fig. 6, which reproduces Fig. 2 of [51], identifies the characteristic V-shape of the resonant structure of the 2-body problem, although the diameter takes similar values in the neighbourhood of the separatrix (similarly to Fig. 5). The benefits of considering $\|\Delta\delta a\|$ over δa are made evident in the dynamical map of the right-hand panel. The V-shape of the separatrix is now undoubtedly identifiable. Each dynamical map comes with its corresponding landscape computed over the dashed line of initial conditions after varying n_1/n_2 but frozen $e = 0.17$. The obtained δa landscape is analogue to the one obtained for the integrable pendulum (recall Fig. 1) and contains 3 points where δa loses its regularity. Two of them correspond to the separatrix crossing (red vertical lines), and the latter corresponds to the crossing of the pericentric branch (green vertical lines at $n_1/n_2 \sim 2$). Whilst δa becomes singular at this point, the numerical values of $\|\Delta\delta a\|$ does not permit to distinguish it sharply. In fact, the $\|\Delta\delta a\|$ landscape contains Dirac pics only for the period ratio corresponding to the separatrix crossing. Consequently, the pericentric branch (or family of stable solutions) is not identifiable.

4.3. The 3-planet case. We now turn our attention to the 3-planet dynamics. The dynamics of these resonant system is governed by the Second Fundamental Model of Resonance. Specific 3-body systems were studied by different means. Let us only mention some of those like the asteroids in the Solar System [47] and exoplanetary systems like TRAPPIST-1 [25, 39] or TOI-178 [37]. A model for zeroth-order 3-body resonances was provided by [50] who also derived a resonance overlap criterion. More recently, [49] generalised the result and has proposed an integrable model for first-order MMRs ($s = 1$). From a numerical perspective, the detailed analysis of the resonant structure has been provided in both [8] and [49].

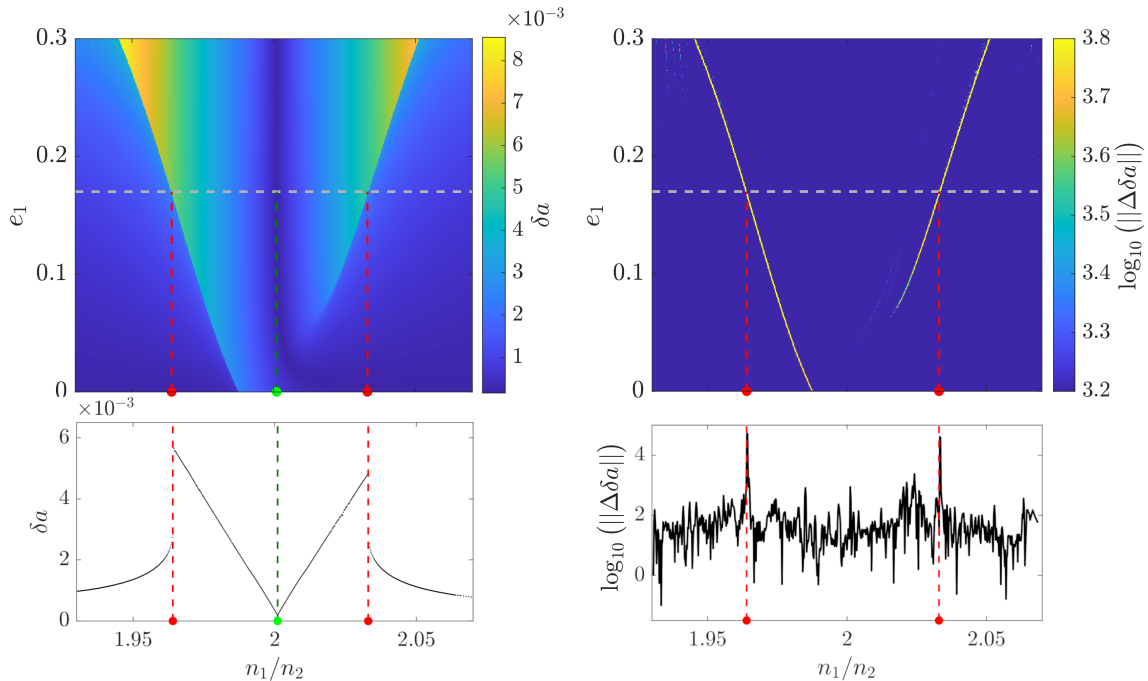


FIGURE 6. (Top left) Dynamical map using δa for the 2/1 MMR in the representative plane $(n_1/n_2, e_1)$ of initial conditions. Planetary masses are $m_1 = 0.05 m_{\text{JUP}}$ and $m_2 = 0.1 m_{\text{JUP}}$ orbiting a central star with mass $M_\star = 1 M_\odot$. Angular variables are initially chosen equal to zero. The pericentric branch of zero-amplitude solutions appears as dark blue, while the regions of maximum variation of the semi-major axis appear in light colours. Total integration time is 10^4 yr. (Bottom left) Landscape of the N -body integration of δa computed over the dashed line of initial conditions at fixed eccentricity $e_1 = 0.17$. (Top right) Corresponding $\|\Delta\delta a\|$ map which clearly identifies the separatrices. (Bottom right) Corresponding landscape of $\|\Delta\delta a\|$.

We retake here the route of [8] and discuss the resonant template through δa computations. We consider a system of three equal mass planets with $m_i = 30$ Earth masses, orbiting a Sun-like star. We adopt the $(n_1/n_2, n_2/n_3)$ representative plane and estimate δa and its Laplacian $\|\Delta\delta a\|$ over a grid of 500×500 initial conditions for 10^4 years (or equivalently, 10^4 orbits of the outer body since it is fixed at $a_3 = 1$ au). The main features observed in the δa map shown in the top panel of Fig. 7 have already been described by [8, 49]. Briefly, the main vertical stripes represent interactions between inner and middle planet, while horizontal lines show the MMRs between middle and outer bodies, and the diagonal curves with negative slope represent commensurabilities between innermost and outermost planets. The diagonal like lines (with positive slopes) are 3-planet zero- and first-order commensurabilities. The connected region of orbits with large δa correspond to either to collisions or escapes. The comparison between the δa and the $\|\Delta\delta a\|$ map (bottom panel of Fig. 7) highlights the striking advantages in considering the $\|\Delta\delta a\|$ indicator. Besides the main structures detected by the δa index, the map contains much more details on secondary structures, and is able to reveal sharply the complex topology of the interacting resonances.

Remark 2. *We underline that the level of details offered by the $\|\Delta\delta a\|$ map is similar to the analysis performed using the well-established MEGNO chaos indicator [10], confer Fig. 2 of [49].*

Remark 3. *The apparent “flatness” of the δa map in Fig. 7 was bypassed by [8] using an analytical procedure, aiming at removing short-period oscillation terms of the semi-major axis (equivalently, the Delaunay variables L), by isolating and recognising the purely periodic components of the disturbing functions. In doing so, the long-term features recognisable in the map were enhanced. Here, the numerical $\|\Delta\delta a\|$ seems to outperform the analytical filtering.*

5. CONCLUSIONS

Dynamics plays a pivotal role in a wide range of scientific and engineering efforts. In planetary sciences, it covers evolution of Solar System’s minor bodies, exoplanetary systems, and ultimately conditions for habitability. Determining the architecture of multi-planetary systems is one of the cornerstones for understanding planet formation and evolution of extrasolar systems as well as our own. The characterisation of extrasolar planets via their dynamics further supplies us with lots of clues hidden in the formation process. Having efficient methods to detect and visualise resonant structures is a key advance in the field. This work has extended and complemented the MEM capabilities by introducing a scalar value inflating hyperbolic structures from their computations. The most important contributions of our work are summarised in the following:

- (1) Celestial mechanics and astrodynamists have been computing Lagrangian Descriptors like quantities for almost 2 decades. We have established an analogy between the M -function, commonly employed in ocean and reaction dynamics, with diameters like quantities such as the MEM employed in gravitational dynamics.
- (2) We have introduced a non-variational dynamical indicator from MEM like computations. The index, complementing further the MEM information, allows to enhance the visualisation of global structures, and improves MEM maps which tend to be “flat.” The key point relies in quantifying the regularity of the diameter metric.
- (3) We applied this new indicator to low-dimensional toy models, allowing to clearly identify separatrices and chaotic seas stemming from stable-unstable manifolds.
- (4) We have presented numerical evidences on the concrete applications and relevance of the method to planetary problems, in the context of mean-motion resonances of the 2 and 3 planets problem. We highlighted the benefits of the tool through dynamical maps, revealing secondary structures otherwise undetected using the MEM.

APPENDIX A. APPLICATION TO A DISCRETE CASE

The framework presented applies also for nearly-integrable discrete systems. For illustrative purpose, following [28], let us consider the 4-dimensional mapping on $\mathbb{T}^2 \times \mathbb{R}^2$ reading

$$(17) \quad \begin{cases} x'_1 = x_1 + y_1, \\ x'_2 = x_2 + y_2, \\ y'_1 = y_1 - \frac{1}{2\pi}(a \sin(2\pi x_1) + c \sin(2\pi(x_1 + x_2))), \\ y'_2 = y_2 - \frac{1}{2\pi}(b \sin(2\pi x_2) + c \sin(2\pi(x_1 + x_2))), \end{cases}$$

where a, b, c are real parameters. When $c = 0$, the mapping is a product of two uncoupled standard-maps. In the following, we consider $a = 0.1$, $b = 0.1$ and $c = 0.07$, and we generate 500×500 initial conditions distributed in the (y_1, y_2) action plane $[-0.25, 0.65]^2$ (fixing $x_1 = x_2 = 0$) iterated up to

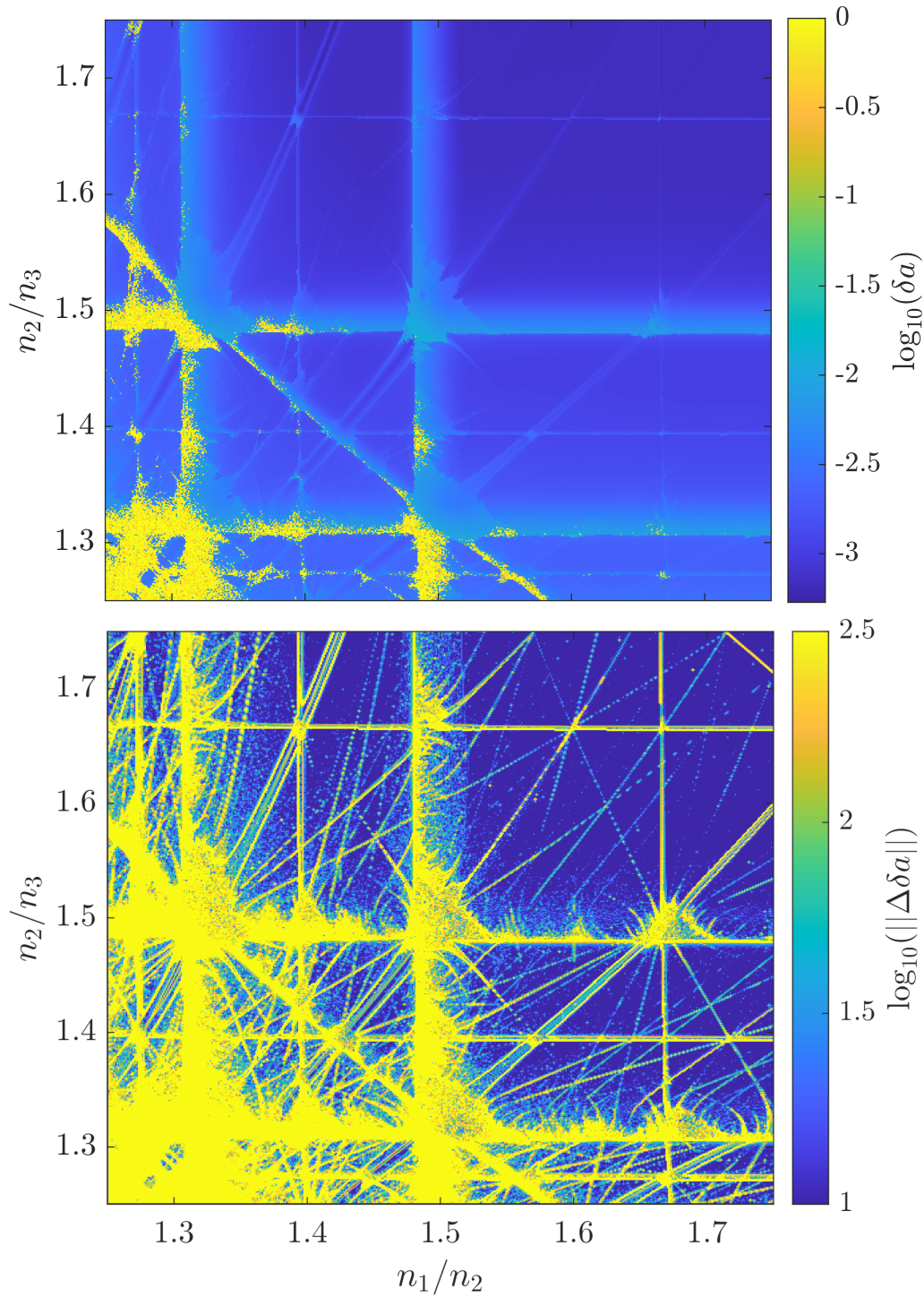


FIGURE 7. Dynamical maps for the 3-planet case in the $(n_1/n_2, n_2/n_3)$ plane with a central star with mass $1 M_\star$ and three planets with equal masses $m = 30 m_\oplus$. The grid consists in 500×500 initial conditions propagated over 10^4 periods of the outer planet (placed at $a_3 = 1$ au). The δa map (top) underestimate the overall resonant and chaotic architecture, and fails in recognising thinner secondary structures as they appear with the $\|\Delta\delta a\|$ analysis (bottom).

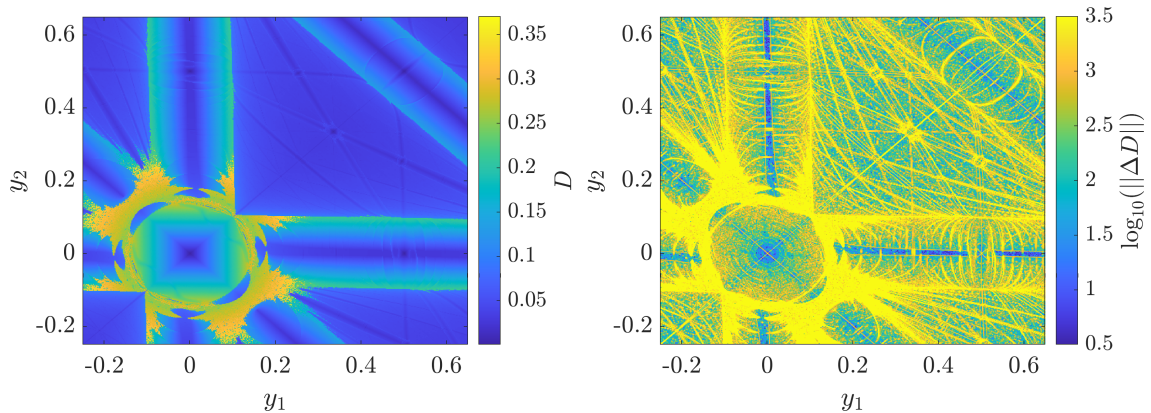


FIGURE 8. Dynamical maps associated to Eq. (17) with $a = 0.1$, $b = 0.1$, $c = 0.07$. Besides revealing the main strips, the $\|\Delta D\|$ index (right-hand side) also highlights smaller resonant strips and chaos in the vicinity of their crossings, otherwise undetected with the diameter metric (left-hand side).

the final time $T = 10^3$. The numerical setting follows closely [28], who dealt with fast Lyapunov indicators [22]. In Fig. 8, we show alternatively the results of the D and $\|\Delta D\|$ analysis to provide a global representation of the phase space. Although the diameter reveal the low order resonant strips, it does not provide clear insights about the geography of lower order resonances, and the distribution of chaotic motions near the resonant crossings. This “flatness” in the map is reinvigorated by the $\|\Delta D\|$ index, which reinvigorates minute details of the geography of low-order resonant structures.

APPENDIX B. ANALYTICAL PROPERTIES OF THE DIAMETER FOR THE PENDULUM MODEL

The non-differentiability of the diameter near the stable equilibrium and its discontinuity when crossing transversally the separatrix of the pendulum (as observed numerically in Fig. 1) are proven analytically.

Proposition 1 (Diameter in elliptic region.). *Let $\mathcal{H}(p, q) = \frac{p^2}{2} + \frac{q^2}{2}$ be the Hamiltonian of the linear oscillator, $(p, q) \in D \subset \mathbb{R}^2$. Then we have*

$$(18) \quad D(p_0, q_0) = 2\sqrt{p_0^2 + q_0^2}.$$

Proof. The system is 1-DoF and integrable. Following [48], we parameterise orbits with their energy levels, thus accounting for an infinitely large time-window. The flow generates circles around the origin with radii

$$(19) \quad r(p_0, q_0) = \sqrt{p_0^2 + q_0^2}.$$

The diameter thus reads

$$(20) \quad D(p_0, q_0) = 2r(p_0, q_0).$$

Along the line of initial condition $q_0 = 0$, one get

$$(21) \quad D(p_0, 0) = 2\sqrt{p_0^2} = 2|p_0|,$$

and in particular D is not differentiable at $p_0 = 0$. □

Proposition 2 (Discontinuity when crossing the separatrix). *Let $\mathcal{H}(p, q) = \frac{p^2}{2} - \cos q$ be the Hamiltonian of the pendulum, $(p, q) \in D \times [-\pi, \pi]$, $D \subset \mathbb{R}$. The diameter is discontinuous on the energy level labelling the separatrix.*

Proof. The librational domain corresponds to the range of energy $E \in [-1, 1)$, the circulatory domain to $E > 1$, and the separatrix has energy $E = 1$. Let E_0 denote the initial energy associated to (p_0, q_0) . The diameter reads

$$(22) \quad D(p_0, q_0) = \begin{cases} 2\sqrt{2(E_0 + 1)}, & E_0 \in [-1, 1), \\ \sqrt{2(E_0 + 1)} - \sqrt{2(E_0 - 1)}, & E_0 > 1, \end{cases}$$

from which follows the discontinuity announced at $E_0 = 1$. □

ACKNOWLEDGMENTS

J.D. is a postdoctoral researcher of the “Fonds de la Recherche Scientifique” - FNRS. C.C. acknowledges FNRS Grant No. F.4523.20 (DYNAMITE MIS-project). It is our pleasure to acknowledge feedback and discussions with Ana Maria Mancho, Elisa Maria Alessi and Timoteo Carletti.

REFERENCES

- [1] Elisa Maria Alessi, Giulia Schettino, Alessandro Rossi, and Giovanni B Valsecchi. Natural highways for end-of-life solutions in the LEO region. *Celestial Mechanics and Dynamical Astronomy*, 130(5):1–22, 2018.
- [2] EM Alessi, Florent Deleflie, AJ Rosengren, Alessandro Rossi, GB Valsecchi, Jerome Daquin, and Klaus Merz. A numerical investigation on the eccentricity growth of GNSS disposal orbits. *Celestial Mechanics and Dynamical Astronomy*, 125(1):71–90, 2016.
- [3] R Alves Silva, Cristian Beauge, S Ferraz Mello, Pablo Miguel Cincotta, and Claudia Marcela Giordano. Instability times in the HD 181433 exoplanetary system. *Astronomy & Astrophysics*, 2021.
- [4] Roberto Barrio. Sensitivity tools vs. Poincaré sections. *Chaos, Solitons & Fractals*, 25(3):711–726, 2005.
- [5] C Beaugé and D Nesvorný. Multiple-planet scattering and the origin of hot Jupiters. *The Astrophysical Journal*, 751(2):119, 2012.
- [6] A Celletti, E Karampotsiou, C Lhotka, G Pucacco, and M Volpi. Laplace-like resonances with tidal effects. *Astronomy & Astrophysics*, 655:A94, 2021.
- [7] C Charalambous, CA Giuppone, and OM Guilera. Web of resonances and possible path of evolution of the small Uranian satellites. *Astrophysics and Space Science*, 367(5):1–15, 2022.
- [8] Carolina Charalambous, Javier Guillermo Marti, Cristian Beauge, and Ximena Soledad Ramos. Resonance capture and dynamics of three-planet systems. *Monthly Notices of the Royal Astronomical Society*, 477(1):1414–1425, 2018.
- [9] B.V Chirikov. A universal instability of many-dimensional oscillator systems. *Physics reports*, 52(5):263–379, 1979.
- [10] Pablo Miguel Cincotta, Claudia Marcela Giordano, and C Simó. Phase space structure of multi-dimensional systems by means of the mean exponential growth factor of nearby orbits. *Physica D: Nonlinear Phenomena*, 182(3-4):151–178, 2003.
- [11] Camilla Colombo and Ioannis Gkolias. Analysis of orbit stability in the geosynchronous region for end-of-life disposal. In *7th European Conference on Space Debris, ESA/ESOC*, pages 1–14. ESA, 2017.
- [12] Galen T Craven and Rigoberto Hernandez. Lagrangian descriptors of thermalized transition states on time-varying energy surfaces. *Physical review letters*, 115(14):148301, 2015.
- [13] Jezabel Curbelo, Carlos R Mechoso, Ana M Mancho, and Stephen Wiggins. Lagrangian study of the final warming in the Southern Stratosphere during 2002: part i. The vortex splitting at upper levels. *Climate Dynamics*, 53(5):2779–2792, 2019.
- [14] Jezabel Curbelo, Carlos R Mechoso, Ana M Mancho, and Stephen Wiggins. Lagrangian study of the final warming in the Southern Stratosphere during 2002: Part ii. 3d structure. *Climate Dynamics*, 53(3):1277–1286, 2019.
- [15] J Daquin, M Pedenon-Orlanducci, M Agaoglou, G Garcia-Sanchez, and M Mancho, A. Global dynamics visualisation from Lagrangian Descriptors. Applications to discrete and continuous systems. *Physica D: Nonlinear Phenomena*, 442:133520, 2022.
- [16] Jérôme Daquin, Ioannis Gkolias, and Aaron J Rosengren. Drift and its mediation in terrestrial orbits. *Frontiers in Applied Mathematics and Statistics*, 4:35, 2018.

- [17] R Dvorak, E Pilat-Lohinger, R Schwarz, and F Freistetter. Extrasolar Trojan planets close to habitable zones. *Astronomy & Astrophysics*, 426(2):L37–L40, 2004.
- [18] Yves Elskens and DF Escande. Infinite resonance overlap: a natural limit for Hamiltonian chaos. *Physica D: Nonlinear Phenomena*, 62(1-4):66–74, 1993.
- [19] Dominique F Escande and Fabrice Doveil. Renormalization method for computing the threshold of the large-scale stochastic instability in two degrees of freedom hamiltonian systems. *Journal of Statistical Physics*, 26(2):257–284, 1981.
- [20] Matthias Feldmaier, Andrej Junginger, Jörg Main, Günter Wunner, and Rigoberto Hernandez. Obtaining time-dependent multi-dimensional dividing surfaces using Lagrangian descriptors. *Chemical Physics Letters*, 687:194–199, 2017.
- [21] Marc Fouchard, Elena Lega, Christiane Froeschlé, and Claude Froeschlé. On the relationship between fast lyapunov indicator and periodic orbits for continuous flows. In *Modern Celestial Mechanics: From Theory to Applications*, pages 205–222. Springer, 2002.
- [22] Claude Froeschlé, Elena Lega, and Robert Gonczi. Fast Lyapunov indicators. Application to asteroidal motion. *Celestial Mechanics and Dynamical Astronomy*, 67(1):41–62, 1997.
- [23] Tabaré Gallardo, Leonardo Coito, and Luciana Badano. Planetary and satellite three body mean motion resonances. *Icarus*, 274:83–98, 2016.
- [24] Víctor J García-Garrido and Stephen Wiggins. Lagrangian descriptors and the action integral of classical mechanics. *Physica D: Nonlinear Phenomena*, 434:133206, 2022.
- [25] Michaël Gillon, Amaury HMJ Triaud, Brice-Olivier Demory, Emmanuël Jehin, Eric Agol, Katherine M Deck, Susan M Lederer, Julien De Wit, Artem Burdanov, James G Ingalls, et al. Seven temperate terrestrial planets around the nearby ultracool dwarf star TRAPPIST-1. *Nature*, 542(7642):456–460, 2017.
- [26] CA Giuppone, P Benítez-Llambay, and C Beaugé. Origin and detectability of co-orbital planets from radial velocity data. *Monthly Notices of the Royal Astronomical Society*, 421(1):356–368, 2012.
- [27] Ioannis Gkolias, Jérôme Daquin, Fabien Gachet, and Aaron J Rosengren. From order to chaos in Earth satellite orbits. *The Astronomical Journal*, 152(5):119, 2016.
- [28] Nathan Guillery and James D Meiss. Diffusion and drift in volume-preserving maps. *Regular and Chaotic Dynamics*, 22(6):700–720, 2017.
- [29] Sam Hadden. An integrable model for the dynamics of planetary mean-motion resonances. *The Astronomical Journal*, 158(6):238, 2019.
- [30] Sam Hadden and Matthew J Payne. Modeling radial velocity data of resonant planets to infer migration histories. *The Astronomical Journal*, 160(3):106, 2020.
- [31] Jacques Henrard and Anne Lemaitre. A second fundamental model for resonance. *Celestial mechanics*, 30(2):197–218, 1983.
- [32] Malcolm Hillebrand, Sebastian Zimper, Arnold Ngapasare, Matthaios Katsanikas, Stephen R. Wiggins, and Charalampos Skokos. Quantifying chaos using Lagrangian descriptors, 2022.
- [33] Andrej Junginger, Lennart Duvenbeck, Matthias Feldmaier, Jörg Main, Günter Wunner, and Rigoberto Hernandez. Chemical dynamics between wells across a time-dependent barrier: Self-similarity in the Lagrangian descriptor and reactive basins. *The Journal of chemical physics*, 147(6):064101, 2017.
- [34] Veselin B Kostov, Jerome A Orosz, Adina D Feinstein, William F Welsh, Wolf Cukier, Nader Haghighipour, Billy Quarles, David V Martin, Benjamin T Montet, Guillermo Torres, et al. TOI-1338: TESS’first transiting circumbinary planet. *The Astronomical Journal*, 159(6):253, 2020.
- [35] J Laskar. Analytical framework in Poincaré variables for the motion of the solar system. In *Predictability, Stability, and Chaos in N-Body Dynamical Systems*, pages 93–114. Springer, 1991.
- [36] Jacques Laskar. Frequency analysis for multi-dimensional systems. Global dynamics and diffusion. *Physica D: Nonlinear Phenomena*, 67(1-3):257–281, 1993.
- [37] Adrien Leleu, Yann Alibert, NC Hara, Matthew John Hooton, TG Wilson, P Robutel, J-B Delisle, J Laskar, S Hoyer, C Lovis, et al. Six transiting planets and a chain of Laplace resonances in TOI-178. *Astronomy & Astrophysics*, 649:A26, 2021.
- [38] Carlos Lopesino, Francisco Balibrea, Stephen Wiggins, and Ana M Mancho. Lagrangian descriptors for two dimensional, area preserving, autonomous and nonautonomous maps. *Communications in Nonlinear Science and Numerical Simulation*, 27(1-3):40–51, 2015.
- [39] Rodrigo Luger, Marko Sestovic, Ethan Kruse, Simon L Grimm, Brice-Olivier Demory, Eric Agol, Emeline Bolmont, Daniel Fabrycky, Catarina S Fernandes, Valérie Van Grootel, et al. A seven-planet resonant chain in TRAPPIST-1. *Nature Astronomy*, 1(6):1–8, 2017.
- [40] JA Jiménez Madrid and Ana M Mancho. Distinguished trajectories in time dependent vector fields. *Chaos: An Interdisciplinary Journal of Nonlinear Science*, 19(1):013111, 2009.
- [41] A.M. Mancho, S. Wiggins, J. Curbelo, and C. Mendoza. Lagrangian descriptors: A method for revealing phase space structures of general time dependent dynamical systems. *Commun Nonlinear Sci Numer Simulat*, 18:3530–3557, 2013.

- [42] James D Meiss. *Differential dynamical systems*. SIAM, 2007.
- [43] C. Mendoza and A.M. Mancho. Hidden geometry of ocean flows. *Physical review letters*, 105(3):038501, 2010.
- [44] Ruty Mundel, Erick Fredj, Hezi Gildor, and Vered Rom-Kedar. New Lagrangian diagnostics for characterizing fluid flow mixing. *Physics of Fluids*, 26(12):126602, 2014.
- [45] Carl D Murray and Stanley F Dermott. *Solar system dynamics*. Cambridge university press, 1999.
- [46] Yutaka Nagahata, Rigoberto Hernandez, and Tamiki Komatsuzaki. Phase space geometry of isolated to condensed chemical reactions. *The Journal of Chemical Physics*, 155(21):210901, 2021.
- [47] D Nesvorný and A Morbidelli. Three-body mean motion resonances and the chaotic structure of the asteroid belt. *The Astronomical Journal*, 116(6):3029, 1998.
- [48] Rémi Pédenon-Orlanducci, Timoteo Carletti, Anne Lemaitre, and Jérôme Daquin. Geometric parametrisation of Lagrangian Descriptors for 1 degree-of-freedom systems. In Carla M.A. Pinto, editor, *Nonlinear Dynamics and Complexity: Mathematical Modelling of Real-World Problems*, pages 221–238. Springer International Publishing, 2022.
- [49] A.C Petit. An integrable model for first-order three-planet mean motion resonances. *Celestial Mechanics and Dynamical Astronomy*, 133(8):1–23, 2021.
- [50] Alice C Quillen. Three-body resonance overlap in closely spaced multiple-planet systems. *Monthly Notices of the Royal Astronomical Society*, 418(2):1043–1054, 2011.
- [51] Ximena Soledad Ramos, Carolina Charalambous, Pablo Benítez-Llambay, and Cristian Beauge. Planetary migration and the origin of the 2: 1 and 3: 2 (near)-resonant population of close-in exoplanets. *Astronomy & Astrophysics*, 602:A101, 2017.
- [52] Ximena Soledad Ramos, Jorge Alfredo Correa-Otto, and Cristian Beauge. The resonance overlap and Hill stability criteria revisited. *Celestial Mechanics and Dynamical Astronomy*, 123(4):453–479, 2015.
- [53] Aaron J Rosengren, Despoina K Skoulidou, Kleomenis Tsiganis, and George Voyatzis. Dynamical cartography of Earth satellite orbits. *Advances in Space Research*, 63(1):443–460, 2019.
- [54] Jean Schneider, Cyrill Dedieu, Pierre Le Sidaner, Renaud Savalle, and Ivan Zolotukhin. Defining and cataloging exoplanets: the exoplanet. eu database. *Astronomy & Astrophysics*, 532:A79, 2011.
- [55] W Sessin and S Ferraz-Mello. Motion of two planets with periods commensurable in the ratio 2: 1 solutions of the hori auxiliary system. *Celestial mechanics*, 32(4):307–332, 1984.
- [56] Ch Skokos. Alignment indices: a new, simple method for determining the ordered or chaotic nature of orbits. *Journal of Physics A: Mathematical and General*, 34(47):10029, 2001.
- [57] Ch Skokos, TC Bountis, and Ch Antonopoulos. Geometrical properties of local dynamics in Hamiltonian systems: The Generalized Alignment Index (GALI) method. *Physica D: Nonlinear Phenomena*, 231(1):30–54, 2007.
- [58] M Stalport, J-B Delisle, S Udry, EC Matthews, V Bourrier, and A Leleu. A general stability-driven approach for the refinement of multi-planet systems. *Astronomy & Astrophysics*, 664:A53, 2022.
- [59] Jean Teyssandier, Anne-Sophie Libert, and Eric Agol. TRAPPIST-1: Dynamical analysis of the transit-timing variations and origin of the resonant chain. *arXiv preprint arXiv:2110.03340*, 2021.

DEPARTMENT OF MATHEMATICS (NAXYS), 61 AVENUE DE BRUXELLES, 5000, NAMUR, BELGIUM
 Email address: `jerome.daquin@unamur.be`

DEPARTMENT OF MATHEMATICS (NAXYS), 61 AVENUE DE BRUXELLES, 5000, NAMUR, BELGIUM
 Email address: `carolina.charalambous@unamur.be`